Turbulence: A Grand Challenge

Rahul Pandit

Centre for Condensed Matter Theory
Department of Physics
Indian Institute of Science
Bangalore, India.

6 February 2010
NESP2010 Satish Dhawan Lecture
Indian Institute of Technology, Kanpur.

References

- Dynamic Multiscaling in Fluid Turbulence : An Overview, D. Mitra and R. Pandit, *Physica A* **318**, 179 (2003).

- Varieties of Dynamic Multiscaling in Fluid Turbulence, D. Mitra and R. Pandit. *Phys. Rev. Lett.* **93**, 024501 (2004).

- Dynamics of Passive-Scalar Turbulence, D. Mitra, and R. Pandit, *Phys. Rev. Lett.* **95**, 144501 (2005).

- Drag reduction by polymer additives in decaying turbulence, C. Kalelkar, R. Govindarajan, and R. Pandit, Phys. Rev. E, **72**, 017301 (2005).

References

- Dynamic Multiscaling in Turbulence, R. Pandit, S.S. Ray, and D. Mitra, *Eur. Phy. J. B*, **64**, 463 (2008).

- The Universality of Dynamic Multiscaling in Homogeneous, Isotropic Navier-Stokes and Passive-Scalar Turbulence, S. S. Ray, D. Mitra, and R. Pandit, *New Journal of Physics*, **10**, 033003 (2008).

- Statistically Steady Turbulence in Thin Films: Direct Numerical Simulations with Ekman Friction, P. Perlekar and R. Pandit, *New Journal of Physics*, **11**, 073003 (2009).

- Statistical Properties of Turbulence: An Overview, R. Pandit, P. Perlekar, and S.S. Ray, *Pramana - Journal of Physics*, **73**, 157 (2009).

- Turbulence-induced melting of a nonequilibrium vortex crystal in a forced thin fluid film, P. Perlekar and R. Pandit, *New Journal of Physics*, in press (2009).

Outline

- Turbulence: Pictures.
- Turbulence: Grand Challenges.
- Multiscaling in homogeneous, isotropic, turbulence:
  - Structure functions;
  - Kolmogorov 1941 - simple scaling;
  - multiscaling and dynamic multiscaling.
- Two-dimensional turbulence in soap films.
- Turbulence with polymer additives.
- Conclusions.

Turbulence in art:

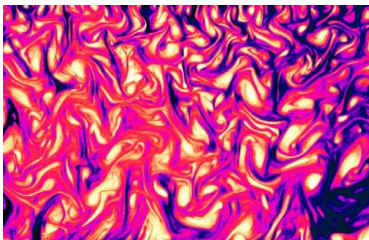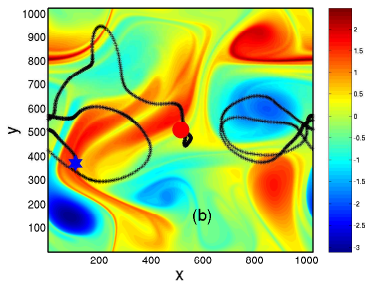Malhar, da Vinci, Hokusai:

Flow behind a comb in a soap film.

Particle trajectories

Lagrangian trajectory in a 2D flow.

Turbulence behind obstacles:

Wake behind two cylinders (top) and homogeneous turbulence behind a grid (bottom).

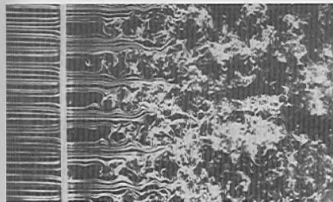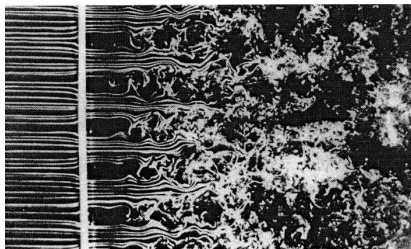Fig. 1.10. Wake behind two identical cylinders at $R = 1800$. Courtesy R. Dumas.

Fig. 1.11. Homogeneous turbulence behind a grid. Photograph T. Corke and H. Nagib.

Decaying, homogeneous and isotropic fluid turbulence, behind a grid.

Use hot-wire anemometry to measure the velocity Reynolds number $Re \equiv \ell U / \nu$.
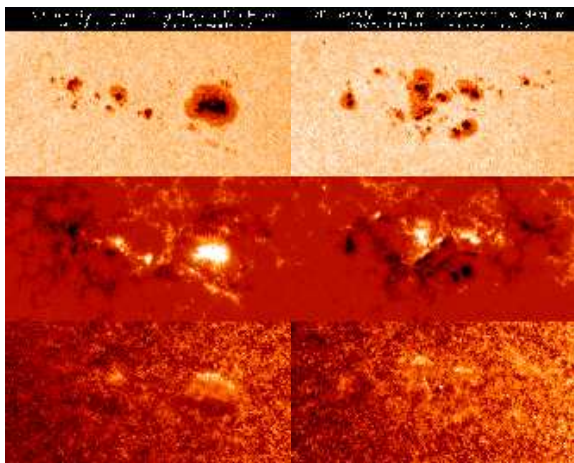
Passive-scalar turbulence:

Turbulent dispersion of small particles:

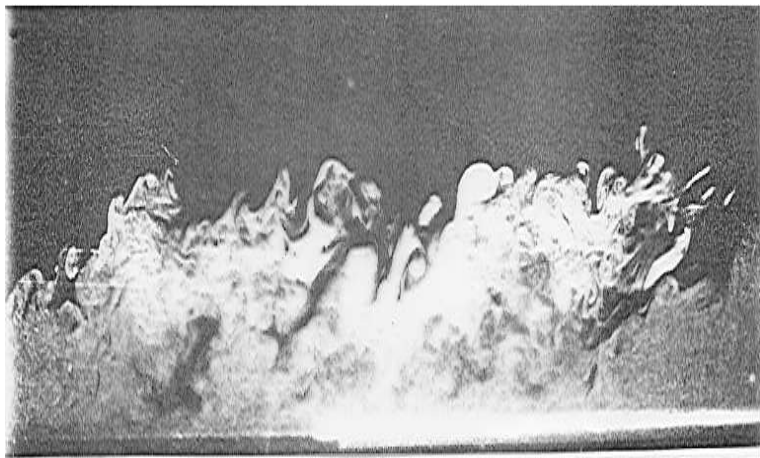

Mount St. Helens on May 18,1980.
http://milou.msc.cornell.edu/lay_turb.html

Turbulence on the sun:

From top to bottom, optical intensity, magnetic field and velocity
as measured by the SOHO project.
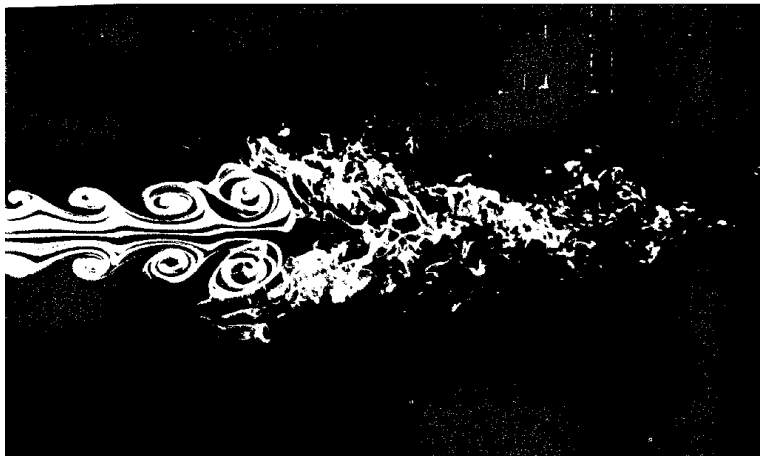http://soi.stanford.edu

Boundary-layer turbulence:

Turbulent boundary layer near a wall ($Re \simeq 4000$), Falco, 1977.
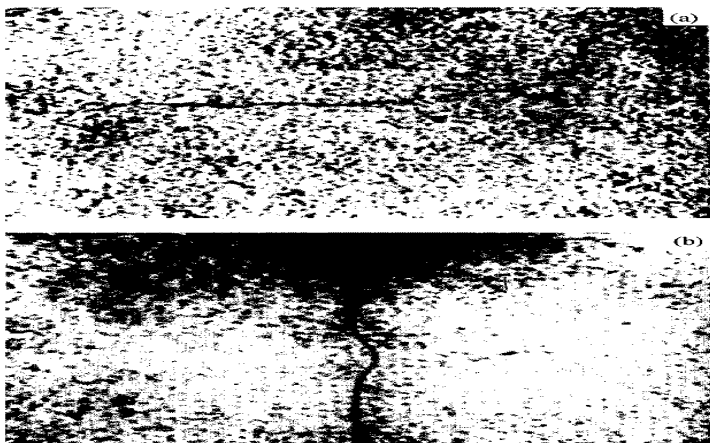
Turbulence in convection:

Plumes in turbulent convection (Sparrow, et al., 1970)

Turbulence in a jet:

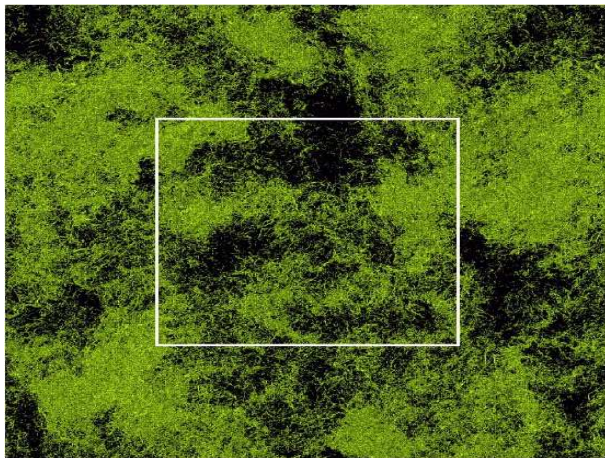Instability of an axisymmetric jet (Drubka and Nagib).

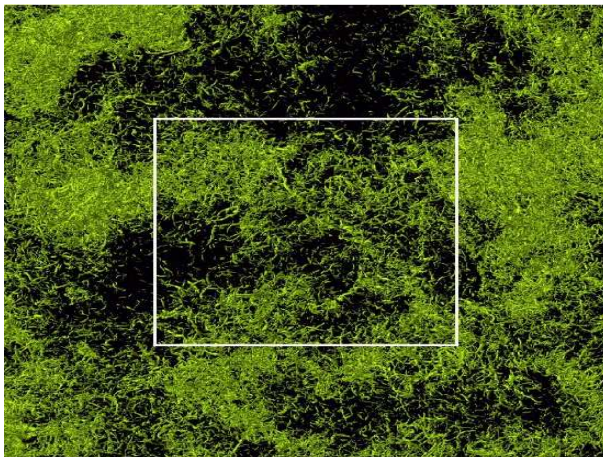# Vorticity filaments in turbulence:

Images of high concentrations of vorticity in water seeded with small bubbles for visualisation.
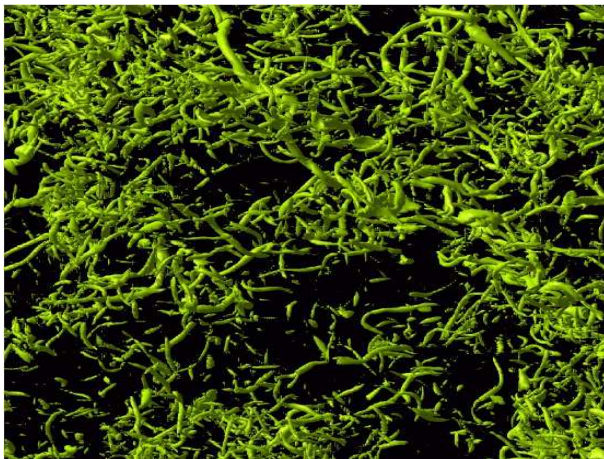
Direct Numerical Simulations (DNS)

Intense-vorticity isosurfaces from a 4096^3 simulation on the Earth Simulator (Y. Kaneda, et al., 2003).

Enlarged view of the inner square region of the previous figure.

Enlarged view of the inner square region of the previous figure.

Challenges

- ▶ Engineers : Characterisation and control of turbulent flows such as flows in pipes or over cars and aeroplanes.
- ▶ Mathematicians : Proofs for the smoothness, or lack thereof, of solutions of the Navier-Stokes and related equations.
- ▶ Challenges also for fluid dynamicists, astrophysicists, geophysicists, climate scientists, plasma physicists ....

We concentrate on the statistical characterisation of fluid turbulence in three dimensions, the turbulence of passive scalars such as pollutants, two-dimensional turbulence in thin films or soap films, and fluid turbulence with polymer additives.

Multiscaling in Fluid and Passive-Scalar Turbulence

- We need a probabilistic description of turbulence (see, e.g., U. Frisch):
- Velocity signals from turbulent flows are disorganised.
- They are unpredictable in their detailed behaviour.
- Some average properties of the signals are quite reproducible.

Lessons

- Large spatial scales: contain most of the energy.
- Small scales: Inertial and dissipation ranges.
- Small scales: Homogeneous and isotropic, to a good approximation (far from boundaries, etc.)
- Inertial-range correlation (or structure functions) exhibit power laws with universal exponents (reminiscent of critical phenomena).

Multiscaling in homogeneous, isotropic, turbulence:

- Structure functions;
- Kolmogorov 1941 - simple scaling;
- multiscaling and dynamic multiscaling;
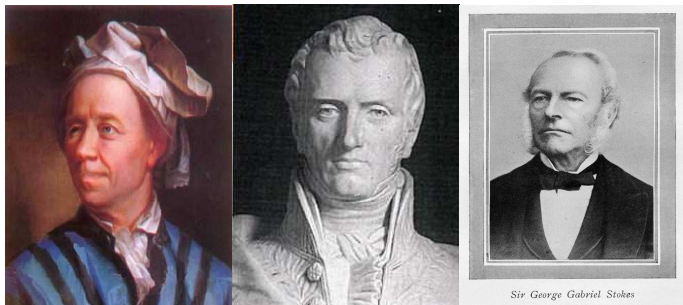- passive-scalar turbulence.

The equations:

- Fluid flows are governed by the Navier-Stokes equation augmented by the incompressibility condition

$$\partial_t \vec{u} + (\vec{u}.\vec{\nabla})\vec{u} = \nu\nabla^2\vec{u} - \vec{\nabla}p/\rho + \vec{f}/\rho;$$

$$\vec{\nabla}.\vec{u} = 0.$$

- $\vec{u}$: Eulerian velocity
- p: pressure
- ν: kinematic viscosity
- ρ: density
- $\vec{f}$: external force

Pioneers

Sir George Gabriel Stokes

Leonhard Euler (1707-1783), Claude-Louis Navier (1785-1836), and George Gabriel Stokes (1819-1903).

Equal-Time Structure Functions

Order-p, equal-time, structure functions:

$$\mathcal{S}_p(r) \equiv \langle [\delta u_\parallel(\vec{x}, \vec{r}, t)]^p \rangle \sim r^{\zeta_p};$$

$$\delta u_\parallel(\vec{x}, \vec{r}, t) \equiv [\vec{u}(\vec{x} + \vec{r}, t) - \vec{u}(\vec{x}, t)] \cdot \frac{\vec{r}}{r};$$

for r in the inertial range $\eta_d << r << L$;

η_d: Kolmogorov dissipation scale;

L: large length scale at which energy is injected into the system;

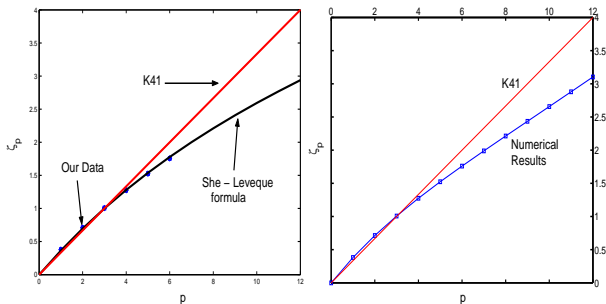energy cascades from L to η_d where it is dissipated.

- Simple-scaling prediction of Kolmogorov: $\zeta_p^{K41} = p/3$ (recall critical-point phenomena).
- Experiments favour multiscaling: ζ_p a nonlinear, convex monotone increasing function of p.

Results: Equal-Time Structure Function

Plots of ζ_p vs p for statistically steady (left) and decaying turbulence (right).

A reasonably good parametrization of experimental and numerical data is provided by the She-Leveque formula.

Eulerian *versus* Lagrangian

- Study of turbulent flows can involve two points of view :
    - **Eulerian** : A description in terms of field variables defined with respect to a frame of reference fixed in space;
    - **Lagrangian** : A description in terms of field variables defined with respect to a frame of reference of fluid particles co-moving with the flow.

Advantages of the Lagrangian description

- Sweeping effect negated – allows for calculation of time-dependent quantities.
- Natural framework for describing transport, diffusion and mixing processes.
- Recent advances in understanding aggregation and clustering.
- Useful framework for modelling.

Equations of motion

- Eulerian :

$$\mathbf{a} = \frac{\partial \mathbf{u}}{\partial t} + \mathbf{u}.\nabla \mathbf{u} = \nu \nabla^2 \mathbf{u} - \frac{\nabla P}{\rho}.$$

- Lagrangian :

$$\mathbf{v}(t) = \frac{d\mathbf{x}(t)}{dt} = \mathbf{u}[\mathbf{x}(t); t].$$

Quasi-Lagrangian

Quasi-Lagrangian velocity field: Defined with respect to the Lagrangian particle, which was at the point $\vec{r}_0$ at time t_0:

$$u_{ql}(\vec{x}, t|\vec{r}_0, t_0) = \vec{u}(\vec{x} + \vec{\rho}(t|\vec{r}_0, t_0), t)$$

where $\vec{u}$ denotes the Eulerian velocity.

- Equal-time exponents equal to Eulerian ones.
- No sweeping effect: Dynamic exponents equal to those for Lagrangian velocities.

Time-Dependent Structure Functions

- The order-p, time-dependent longitudinal structure function:

$$\mathcal{F}_p(r, \{t_1, \ldots, t_p\}) \equiv \langle [\delta u_\parallel(\vec{x}, t_1, r) \ldots \delta u_\parallel(\vec{x}, t_p, r)] \rangle$$

For simplicity we consider $t_1 = t$ and $t_2 = \ldots = t_p = 0$.

- Given $\mathcal{F}(r, t)$, different ways of extracting time scales yield different exponents that are defined via dynamic-multiscaling ansätze:

$$\mathcal{T}_p(r) \sim r^{z_p}.$$

Integral Time Scale

- From the longitudinal, time-dependent, order-p structure functions, the order-p, degree-M, integral time scale is defined as,

$$\mathcal{T}_{p,M}^{I}(r) \equiv \left[\frac{1}{\mathcal{S}_p(r)} \int_0^\infty \mathcal{F}_p(r,t) t^{(M-1)} dt \right]^{(1/M)}$$

- The integral dynamic multiscaling exponent $z_{p,M}^{I}$ is defined as

$$\mathcal{T}_{p,M}^{I}(r) \sim r^{z_{p,M}^{I}}.$$

Derivative Time Scale

- Similarly, the order-p, degree-M derivative time scale is defined as

$$\mathcal{T}_{p,M}^{D}(r) \equiv \left[\frac{1}{\mathcal{S}_p(r)} \frac{\partial^M \mathcal{F}_p(r,t)}{\partial t^M} \right]^{(-1/M)}$$

- The derivative dynamic multiscaling exponent $z_{p,M}^{D}$ is defined as

$$\mathcal{T}_{p,M}^{D}(r) \sim r^{z_{p,M}^{D}}.$$

Theoretical Prediction

▶ The multifractal model predicts the following bridge relations:

$$z_{p,M}^{I} = 1 + \frac{[\zeta_{p-M} - \zeta_p]}{M};$$

$$z_{p,M}^{D} = 1 + \frac{[\zeta_p - \zeta_{p+M}]}{M}.$$

Integral Time Scales
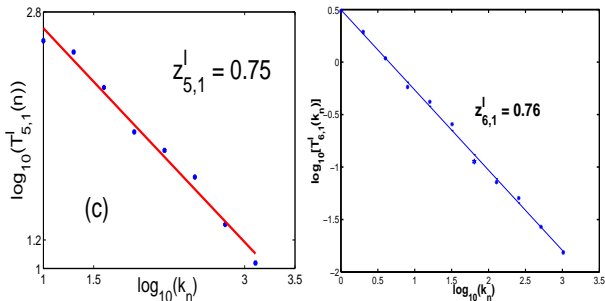
Log-log plots of integral times for statistically steady (left) and decaying (right) turbulence for order-p structure functions; the slopes of these graphs yield $z^I_{p,1}$. The integration is carried out over time 0 to t_u, where we choose t_u such that $F_p(n, t_u)$ (or $Q_p(n, t_u)$) = α for all n and p.

Derivative Time Scales
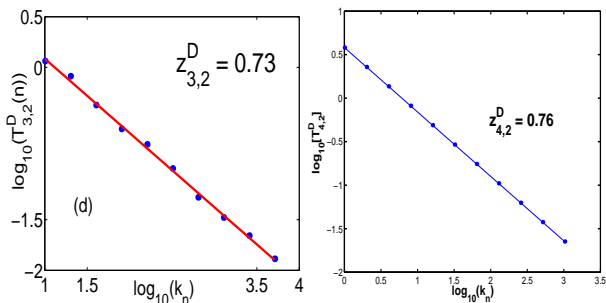
The analogue of the previous figure for derivative time scales yields $z_{p,1}^{D}$. We use a centered, sixth-order, finite-difference scheme by extending $F_p(n, t)$ (or $Q_p(n, t)$) to negative t via $F_p(n, -t)$ (or $Q_p(n, -t)$) $= F_p(n, t)$ (or $Q_p(n, t)$) to obtain the derivative time scales.

- Simple dynamic scaling for Eulerian-velocity structure functions ($z_p^E = 1$).

- Dynamic multiscaling is obtained for Lagrangian or Quasi-Lagrangian structure functions.

- Dynamic multiscaling exponents z_p depend on how $\mathcal{T}_p(r)$ is extracted.

- z_p is related to the equal-time exponents via bridge relations.

- Universality of dynamic exponents: the same for decaying and statistically steady turbulence.

Possible Experimental Verification

- Eulerian velocity : $u(x, t)$
- Lagrangian velocity : $v(x, t_0|t)$
- Define :
  $$\delta v(r, t_0|t) = v(x + r, t_0|t) - v(x, t_0|t)$$
- Construct the time-dependent structure function :
  $$F_p(r, t_0, t_1, ...t_p) \equiv \langle \delta v(r, t_0|t_1)...\delta v(r, t_0|t_p) \rangle$$
- $\langle ... \rangle$ denote averaging over different pairs of particles; the position of each pair at time t_0 is characterised by x_i and $x_i + r$, where i runs from 1 to N (the number of particles).

Passive Scalars

- Passively advected scalars are governed by the advection-diffusion equation

$$\frac{\partial \theta}{\partial t} + \vec{u}.\vec{\nabla}\theta = \kappa \nabla^2 \theta + f_\theta.$$

- We use two different kinds of velocity fields in the advection-diffusion equation for both statistically steady and decaying turbulence:
    - Model A : The Kraichnan ensemble where each component of **u** is a zero-mean, delta-correlated Gaussian random variable.
    - Model B : Velocities from the GOY shell model.

Model A

- The covariance of the field is

$$< u_i(\mathbf{x}, t) u_j(\mathbf{x} + \mathbf{r}, t') >= 2 D_{ij} \delta(t - t')$$

In the limits $L \longrightarrow \infty$ and $\eta \longrightarrow 0$, D_{ij} in real space is

$$D_{ij}(\mathbf{r}) = D^0 \delta_{ij} - \frac{1}{2} d_{ij}(\mathbf{r}))$$

where,

$$d_{ij} = D_1 r^\xi \big[(d - 1 + \xi) \delta_{ij} - \xi \frac{r_i r_j}{r^2} \big]$$

- This model shows multiscaling for equal-time passive-scalar structure functions for $0 < \xi < 2$.
- No dynamic multiscaling.

Multifractal model predicts:

- $z_{p,M}^{D} = 1 - \zeta_{M}^{u}/M$
- $z_{p,M}^{I} = 1 - |\zeta_{-M}^{u}|/M$
- Breakdown of simple scaling.
- Do structure functions with negative exponents exists?

Results: Equal-Time Structure Functions
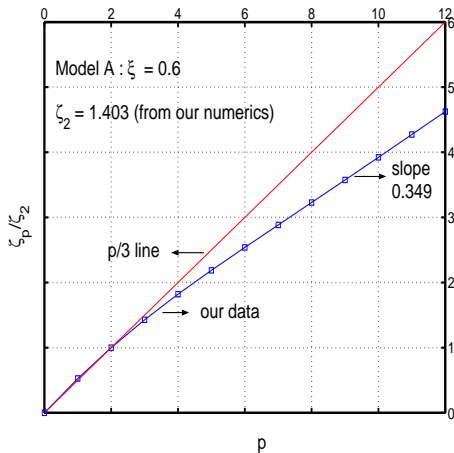
The figure shows the plot of $\frac{\zeta_p}{\zeta_2}$ vs p for model A.

Results: Equal-Time Structure Functions
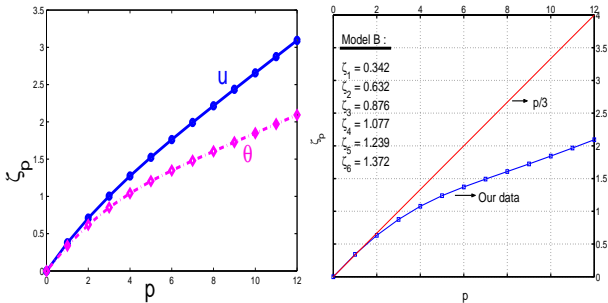
The panel shows plots of ζ_p vs p for model B for statistically steady (right) and decaying (left) turbulence. For comparison, on the left we plot equal-time exponents for both the velocity field (ζ_p^u) and the passive-scalar field (ζ_p^θ).
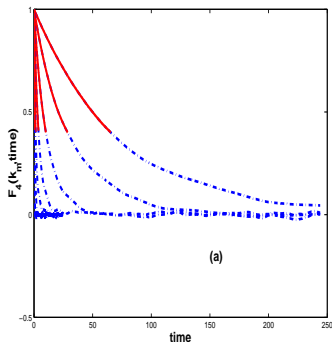
A plot of the fourth-order structure function ($\xi = 0.6$) *vs* time for statistically steady turbulence. The scaling exponent is extracted from the decay constant of the curves.
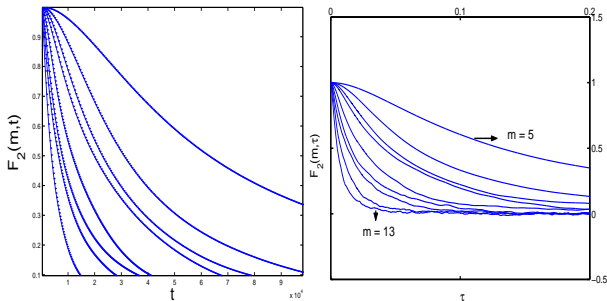
Plots of the second-order time-dependent structure function
vs **the dimensionless time for statistically steady (left) and decaying turbulence (right).**

Model B: Integral Time Scale
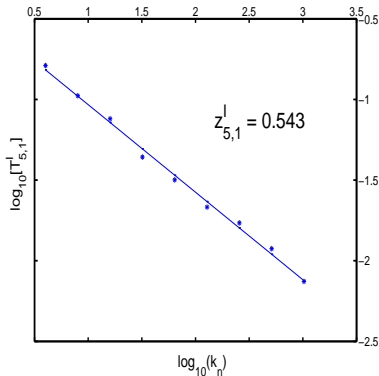
A log-log plot of the integral time scale *vs* the wave-vector in decaying turbulence. The linear fit gives us the scaling exponent $z_{p,M}^{I}$.

Derivative Time Scale
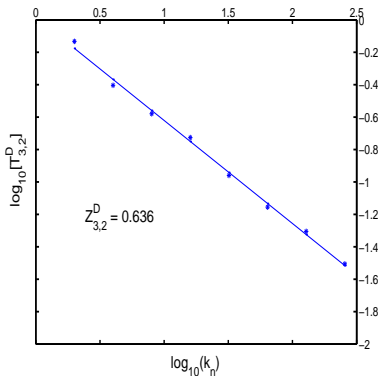
A log-log plot of the derivative time scale *vs* the wave-vector in decaying turbulence. The linear fit gives us the scaling exponent $z_{p,M}^D$.

Two-dimensional turbulence in soap films.

Two-dimensional turbulence:

- Study of high-Reynolds-number solution of the incompressible Navier-Stokes equations:

$$D_t\mathbf{u} = -\nabla p + \nu\nabla^2\mathbf{u}, \tag{1}$$
$$\nabla.\mathbf{u} \equiv 0$$

or

$$\begin{aligned}
D_t\omega &= \nu\nabla^2\omega, \\
\nabla^2\psi &= \omega, \\
\omega &\equiv \nabla \times \mathbf{u}, \\
u_x &= -\partial_y\psi, \\
u_y &= \partial_x\psi.
\end{aligned} \tag{2}$$

- No vortex stretching, $\omega.\nabla\mathbf{u}$ is absent.

Conservation laws:

- Energy conservation in the inviscid, unforced limit.

$$\partial_t E = -2\nu\Omega, \tag{3}$$

$$E = 1/2 \int_{\mathbf{x} \in R^3} |\mathbf{u}|^2,$$

$$\Omega = 1/2 \int_{\mathbf{x} \in R^3} |\omega|^2, \tag{4}$$

- Enstrophy conservation in the inviscid, unforced limit.

$$\partial_t \Omega = -2\nu P, \tag{5}$$

$$P = 1/2 \int_{\mathbf{x} \in R^3} |\nabla \times \omega|^2. \tag{6}$$

Cascades

[Kraichnan, Phys. Fluids, **10**, (1967*a*), Batchelor, Phys. Fluids Suppl. *II*, **12**, (1969)]

- ▶ Energy injected at a length scale l_{inj} will inverse-cascade to large length scales with $E(k) \sim k^{-5/3}$.
- ▶ Energy injected at a length scale l_{inj} will forward-cascade to small length scales with $E(k) \sim k^{-3}$.
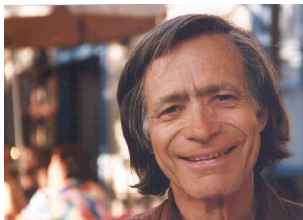
Electromagnetically forced soap films

[M. Rivera, Ph.D. Thesis, arXiv:physics/010305v1]
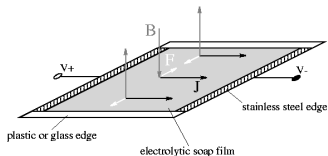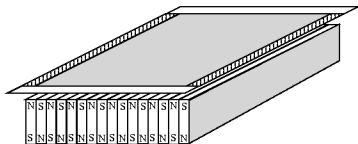
- ▶ Soap film: 400*ml* distilled water + 40*ml* glycerol + 5*ml* commercial liquid detergent,
- ▶ The soap film is suspended on a rectangular frame,
- ▶ The magnetic array produces a Kolmogorov forcing $F_x = F_0 sin(k_y y)$.

Modelling soap films: Incompressible limit

[Chomaz et al., PRA, **41**, (1990), Chomaz, JFM, (2001), P. Fast, arXiv:physics/0511175v1, (2005).]

- Mach Number $M_e \equiv u_{rms}/c$, where c is the speed of the sound in the soap films. For the experiments with electromagnetically forced soap films $M_e \sim 0.06$.

- To leading order soap-film behaviour is governed by the Navier-Stokes(NS) equations in two dimensions + an air drag

$$D_t \mathbf{u} = \nu \nabla^2 \mathbf{u} - \nabla p - \alpha \mathbf{u},$$
$$\nabla \cdot \mathbf{u} = 0.$$

- $D_t \equiv \partial_t + \mathbf{u} \cdot \nabla$, $p \equiv$ pressure, and $\mathbf{u} \equiv$ the velocity

- Vorticity-streamfunction formulation:

$$
\begin{aligned}
D_t \omega &= \nu \nabla^2 \omega - \alpha \omega, \\
\nabla^2 \psi &= \omega, \\
u_x &= -\partial_y \psi, \, u_y = \partial_x \psi.
\end{aligned}
$$

- Incompressibility satisfied by construction.
- No-slip boundary condition on the walls.

DNS for forced soap films:

- Impose the Kolmogorov forcing $F_y = F_0 \sin(k_x x)$ at all times.
- Study the evolution of the energy E and the dissipation rate ϵ with α and ν.
- Study velocity and vorticity structure functions.
- Study the topological properties via PDFs of the Weiss parameter Λ.

Evolution of energy and dissipation

Time evolution of $E(t)/E'$ [(a) and (b)], $\epsilon(t)/\epsilon'$ [(c) and (d)], and $\epsilon_e(t)/\epsilon'$ [(e) and (f)].
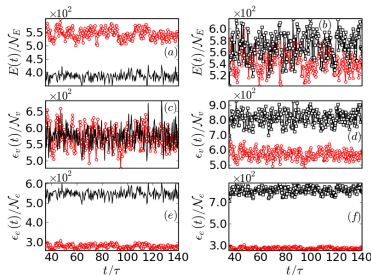
In (a), (c), and (d) we keep $\mathcal{G}$ fixed and vary γ ($\gamma = 0.25$(red lines with circles) and $\gamma = 0.71$(black line)). In (b), (d), and (f) we maintain $Re \simeq 21.2$ and vary γ ($\gamma = 0.25$(red lines with circles) and $\gamma = 0.71$(black line with squares)).
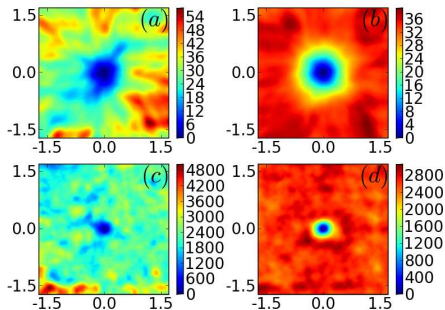
Pseudocolor plots of (a) $S_2(\mathbf{r_c}, \mathbf{R})$, for $\mathbf{r_c} = (2,2)$, (b) $S_2(R)$ (average of $S_2(\mathbf{r_c}, \mathbf{R})$ over $\mathbf{r_c}$), (c) $S_2^{\omega}(\mathbf{r_c}, \mathbf{R})$, for $\mathbf{r_c} = (2,2)$, and (d) $S_2^{\omega}(R)$ (average of $S_2^{\omega}(\mathbf{r_c}, \mathbf{R})$ over $\mathbf{r_c}$).
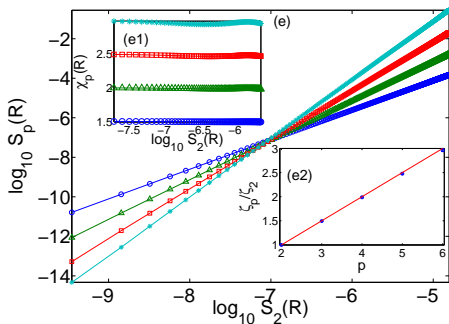
Velocity Structure Functions
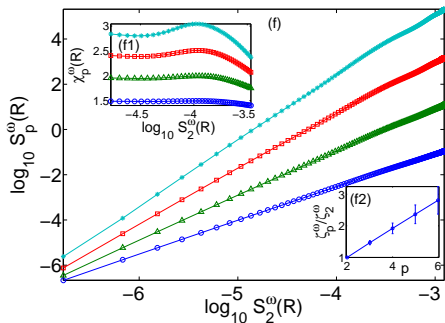
Distribution of centers and saddles

A. Okubo, Deep-Sea Res. **17**, 17 (1970),
J. Weiss, Physica, **48D**, 273 (1991).

▶ Local flow topology determined by

$$\Lambda \equiv \left| \begin{array}{cc} \partial_x u_x & \partial_x u_y \\ \partial_y u_x & \partial_y u_y \end{array} \right| \text{ and}$$

$D \equiv \nabla \cdot \mathbf{u}$

▶ For incompressible flows, $D = 0$

▶ $\Lambda = (\omega^2 - \sigma^2)/4$, $\omega^2 \equiv \sum_{i,j}(\partial_i u_j - \partial_j u_i)^2/2$,
$\sigma^2 \equiv \sum_{i,j}(\partial_i u_j + \partial_j u_i)^2/2$.

▶ At a point (x, y), $\Lambda(x, y) > 0 \implies$ centers, and
$\Lambda(x, y) < 0 \implies$ saddles.

ψ and Λ
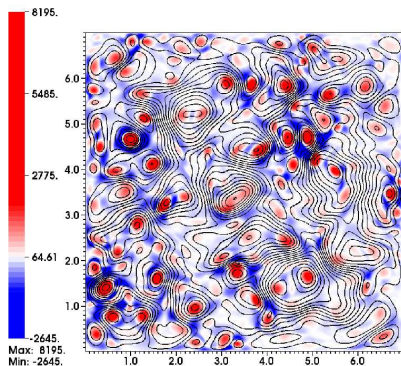
- Contours of ψ overlayed on the pseudocolor plot of Λ.
- $\Lambda > 0$(centers)
- $\Lambda < 0$(saddles)

PDF of Λ: fixed Re
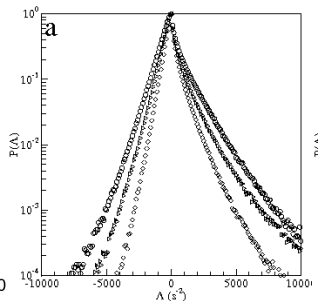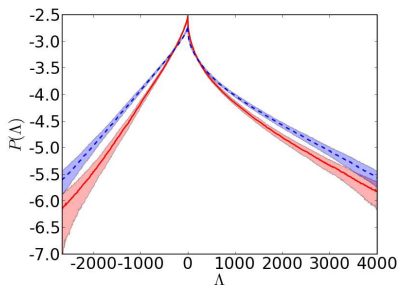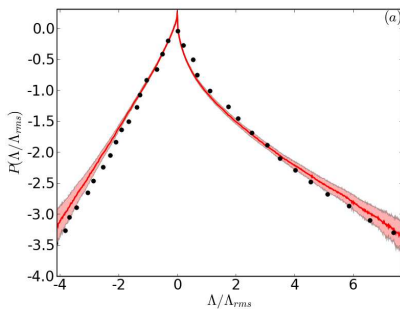

- runs R4 and R6
- Left: Our DNS. $\gamma = 0.25(red)$, $\gamma = 0.71(blue)$.
- Right: Experiments. $\gamma = 0.28(diamond)$, $\gamma = 0.56(triangle)$, $\gamma = 0.97(circle)$.
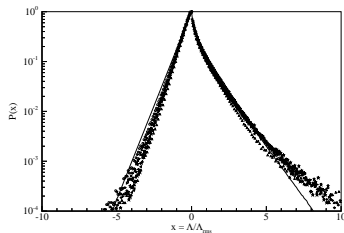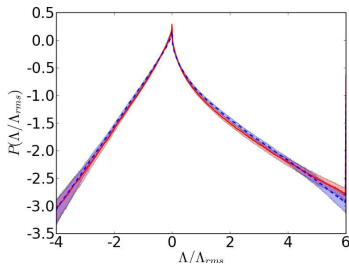
- runs R4 and R6
- PDF normalized by Λ_{rms}.
- Left: Our DNS. $\gamma = 0.25 (red)$, $\gamma = 0.71 (blue)$.
- Right: Experiments. $\gamma = 0.28$(diamond), $\gamma = 0.56$(triangle), $\gamma = 0.97$(circle).

- Our DNS: Red dotted line.
- Experiments: Black dots (op. cit. Rivera et al.).

Multiscaling and quasi-Lagrangian Structure Functions

- Multiscaling in equal-time, Eulerian vorticity structure functions.

- Investigating dynamic-multiscaling in time-dependent, quasi-Lagrangian vorticity structure functions.

- Tracking a single particle in a $2D$ flow with Ekman friction to generate quasi-Lagrangian fields.

Movie

Equal-time Structure Functions for Eulerian and quasi-Lagrangian Fields
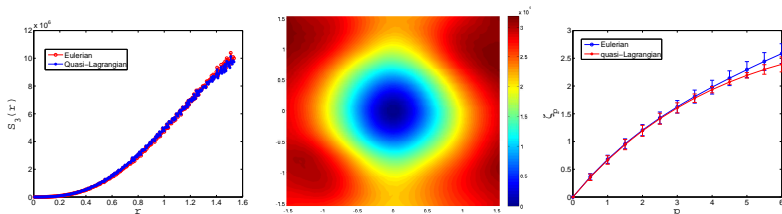
- ▶ Left : Third-order, equal-time vorticity structure functions for Eulerian and quasi-Lagrangian fields.
- ▶ Middle : $S_3^{\omega}(\mathbf{R})$ for the quasi-Lagrangian field, obtained by averaging over the centers r_c.
- ▶ Right : Scaling exponents for equal-time, vorticity structure functions, for both the Eulerian and quasi-Lagrangian fields.
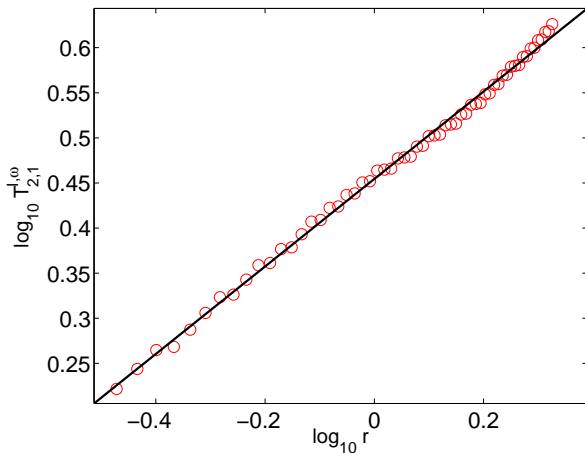
A loglog plot of $T_{2,1}^I$ versus the separation r; the data points are shown by open red circles and the straight black line shows the line of best fit in the inertial range.

- The 2D Navier-Stokes equations with Ekman friction is a good model to describe 2D turbulence in soap-films.
- The topological properties of 2D turbulence in our DNS are the same as those observed in experiments.
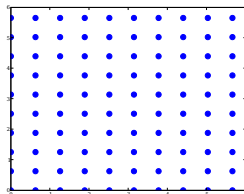- Differences between constant $\mathcal{G}$ and constant Re ensembles explored.

Turbulence induced melting

Statistical Physics: Phase transition

- Solid: Atoms arranged on an lattice.
- Liquid: No ordering of atoms.
- Increasing temperature leads to a transition from solid to a liquid phase. Crystalline phase destroyed on increasing temperature.

Crystal

Liquid
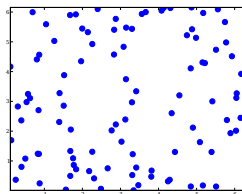
- We use the above ideas to study a similar nonequilibrium transition.

ρ is a periodic function of $\mathbf{r}$:

$$\rho(r) = \sum_{\mathbf{G}} \rho_{\mathbf{G}} \exp(\iota \mathbf{G} \cdot \mathbf{r});$$

- ▶ **G**: of the reciprocal lattice vectors.
- ▶ RY Theory: $\rho_{\mathbf{G}}$ are the order parameters.

Equilibrium Melting

- Spatial correlations: $G(r) = \overline{\langle \rho(\mathbf{x})\rho(\mathbf{x}+\mathbf{r})\rangle}$, where angular brackets denote Gibbsian thermal averages and the overline denotes spatial averaging.

- The Fourier transform of $G(r)$ is related to the static structure function $S(k)$.

Motivation
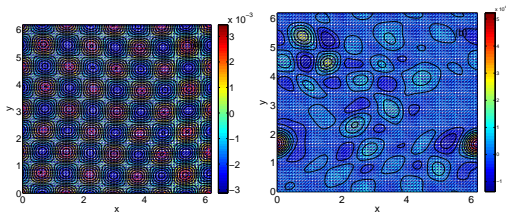
- ▶ Λ field in the laminar state.
- ▶ Λ field in the turbulent state.
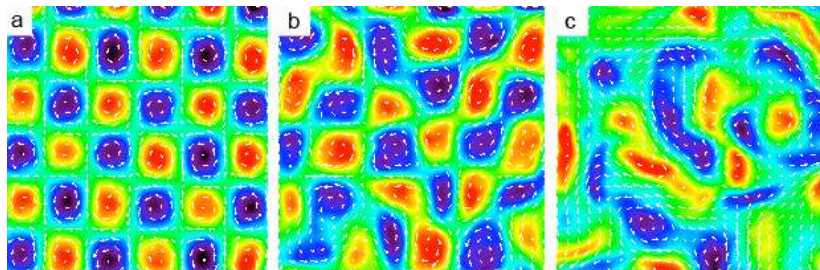
Experiments: Transition to turbulence

[N.T. Ouellete and J.P. Gollub, Phys. Rev. Lett. **99**, 194502 (2007).]
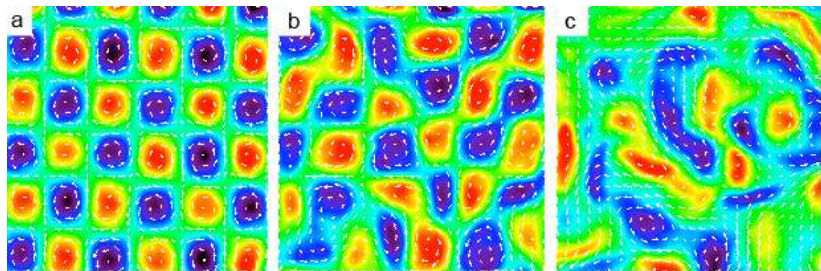
- ▶ Figs. [(a), (b), and (c)] are the snapshots of the stream-function obtained by particle tracking.
- ▶ At Reynolds number $Re \leq Re_c$, two-dimensional lattice with a lattice-spacing of forcing magnets is formed.
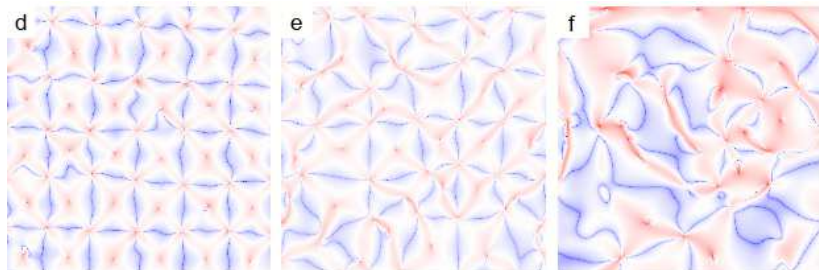
Experiments: Transition to turbulence

[N.T. Ouellete and J.P. Gollub, Phys. Rev. Lett. **99**, 194502 (2007).]

- ▶ On increasing the $Re > Re_c$, the fluid undergoes transition and the lattice distorts.
- ▶ At very high Reynolds number $Re >> Re_c$, turbulence sets in and the underlying lattice is completely destroyed.
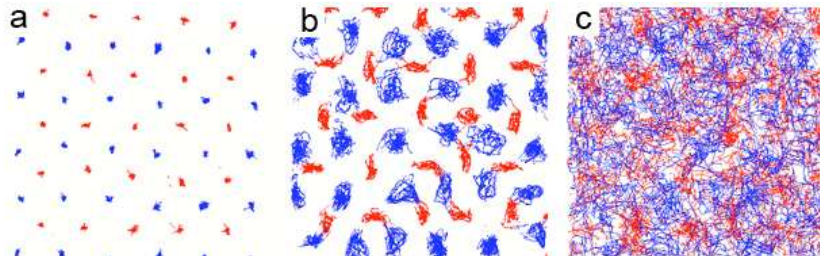
Experiments: Transition to turbulence

[N.T. Ouellete and J.P. Gollub, Phys. Rev. Lett. **99**, 194502 (2007).]

- ▶ Use local-curvature of the Lagrangian trajectories and the Weiss criterion to find the saddles and the centers of the flow Figs. [(d)], (e) and (f)].

Experiments: Transition to turbulence

- ▶ Crsytalline state(Fig. (a)): Particles remain localized.
- ▶ Fig. (b): The particles start to fluctuate around their mean positions as *Re* increases.
- ▶ Melt state (Fig. (c)): In turbulent state, particles are not localized.

[N.T. Ouellete and J.P. Gollub, Phys. Rev. Lett. **99**, 194502 (2007).]

Pair-correlation of the topological special points.

- $g(r) = \frac{V}{N^2} \langle \sum_i \sum_{j \neq i} \delta(\mathbf{r} - \mathbf{r}_{ij}) \rangle$, where V is the volume, and N are the number of particles.
- Laminar(Red square), Intermediate(Green circles), and Chaotic regime (Blue triangle).

Braun et al.

- ▶ Equation: $D_t \omega = \nabla^2 \omega + 2fk \sin(kx) \sin(ky)$, $k = 8$,
- ▶ Observe formation of large scale structures,
- ▶ Control parameter f (Grashof number),
- ▶ Boundary condition: Periodic.

Earlier Numerical Simulations

[M. Brons, A. Skajaa, and O. Skovgaard, arXiv:0806.4757v1]

- ▶ Closely mimic the experiments of Ouellete et al., ibid.; circular domain with no-slip boundaries.
- ▶ Forcing: Eight stirrer with forcing amplitudes $f = K \frac{3r_0 r^2}{r_0^3 + 2r^3}$
  where r_0 is the width of the stirrer, r is the distance from the stirrer, and K is the forcing strength.
- ▶ Simulation done using Finite-element code COSMOL(http://www.comsol.com/).

Our Direct Numerical Simulation(DNS)

- Vorticity-streamfunction formulation
- $f = f_0[sin(kx) + sin(ky)]$
- Normalization

$$
\begin{aligned}
D_t\omega &= \frac{1}{\Omega}\nabla^2\omega - \frac{n^2\gamma}{\Omega}\omega + \frac{n^2}{\Omega}f, \\
\nabla^2\psi &= \omega, \\
\mathbf{u} &= (-\partial_y\psi, \partial_x\psi).
\end{aligned}
$$

- $\mathbf{x}' \to k\mathbf{x}/n$, $t' \to f_0 t/(nk\nu)$, $\omega' \to (nk\nu/f_0)\omega$, and $\mathbf{u}' \to (\nu k^2/f_0)\mathbf{u}$.
- $\Omega \equiv nf_0/(\nu^2 k^3) \equiv nRe$.
- Incompressibility satisfied by construction.

Our Goal

- Study the transition to turbulence as a function of n and Ω.

- Use the Weiss parameter (Λ) as an analog of the crystal density field (ρ) in a conventional crystal.

- Study the two-dimensional spectrum $E_\Lambda(\mathbf{k}) = \Lambda_{\mathbf{k}} \Lambda_{-\mathbf{k}}$ is our analog of $S(k)$.

- Study the autocorrelation function $G(r) = \langle \Lambda(\mathbf{x}) \Lambda(\mathbf{x} + r) \rangle$ in laminar and chaotic regime.

- We also use non-linear dynamics measures such as the Poincare section and the power spectrum of the time-series to characterize the transition.

Direct Numerical Simulation(DNS)

- ▶ Time marching by second-order Runge-Kutta scheme.
- ▶ Derivative and convolution using pseudo-spectral method.

Direct Numerical Simulation(DNS)

- $N = 64, 128, 256$
- Set $\gamma = 0$ unless specified otherwise.
- Vary Ω for fixed n and monitor the transition to turbulence.

Results

Results for n=4

	n	Ω	Comments
R4 − 1	4	$\Omega < \Omega_s$	Square array
R4 − 2	4	$\Omega_s < \Omega \le 6.5$	Steady state, large structures
R4 − 3	4	$\Omega = 8.202$	Periodic orbit
R4 − 4	4	$9.05 < \Omega < 15.3$	Steady state, large structures
R4 − 5	4	$15.3 < \Omega < 17.3$	Periodic orbits
R4 − 6	4	$\Omega = 17.8$	Quasi − periodic + chaos
R4 − 7	4	$\Omega \ge 18.3$	Chaotic

Table: Table indicating the values of Ω and the route to chaos observed in our simulations.

$\Omega = 6.5$: ψ, Λ, and E_Λ
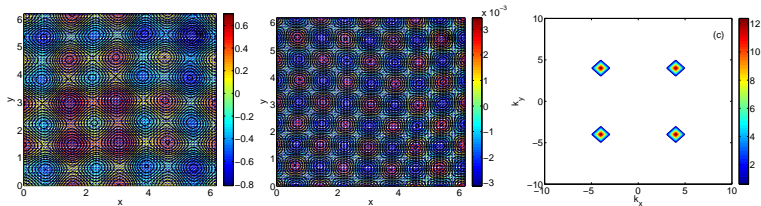
- Steady state.
- Pseudocolor plots of ψ(Left), Λ(Middle), and E_Λ(Right).
- Note the formation of large scale structure in ψ.
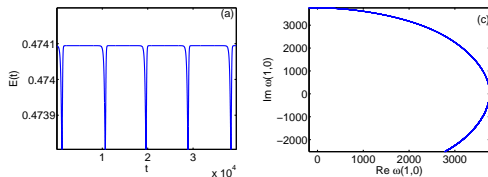
- The time evolution of the energy $E(t)$.
- Plot of projection of the trajectory on the Fourier plane made by velocities $Re[\hat{\omega}(1,1)]$ versus $Im[\hat{\omega}(1,1)]$.
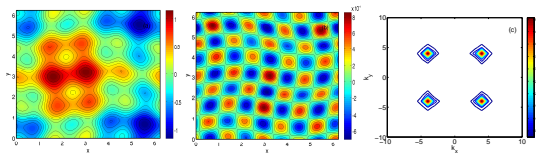
Pseudocolor plots of:

- the streamfunction field
- the Λ field with superimposed contour lines
- the reciprocal space energy spectrum E_Λ.

$\Omega = 11.3$: ψ, Λ, and E_Λ
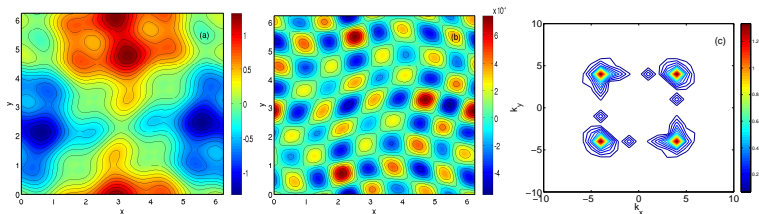
- ► New steady state.
- ► (Left) Pseudocolor plot of ψ.
- ► (Middle) Pseudocolor plot of Λ.
- ► (Right) Pseudocolor plot of the reciprocal space energy spectrum E_Λ.
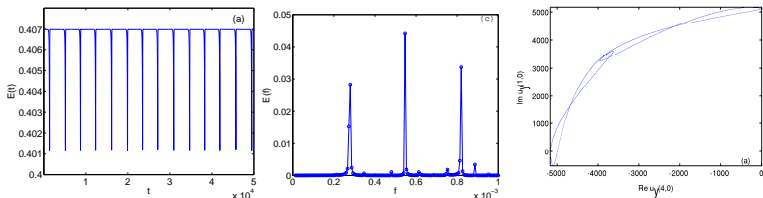
- New periodic state.
- (Left) The time evolution of the energy,
- (Middle) The frequency spectrum of the energy, and
- (Right) The plot of projection of the trajectory on the Fourier plane made by velocities $Re[\hat{u}_y(1,1)]$ versus $Im[\hat{u}_y(1,1)]$.
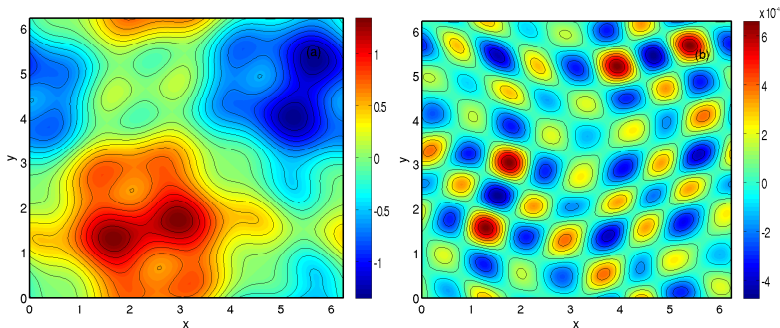
- (Left) Pseudocolor plot of ψ.
- (Right) Pseudocolor plot of Λ.
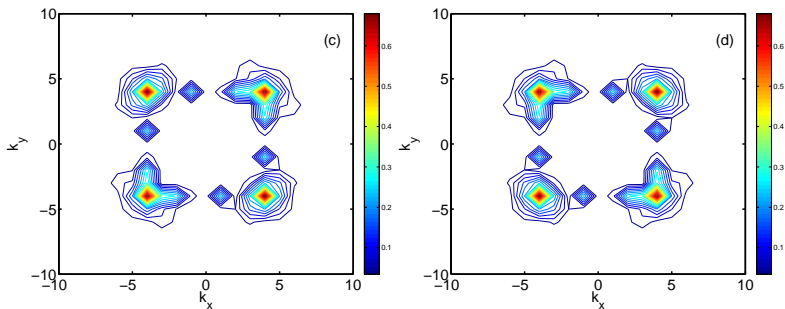
- (Left) E_Λ at the minima of $E(t)$.
- (Right) E_Λ at the maxima of $E(t)$.
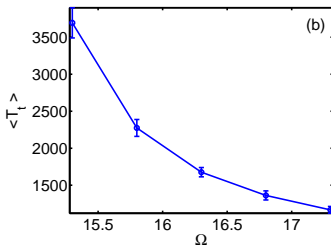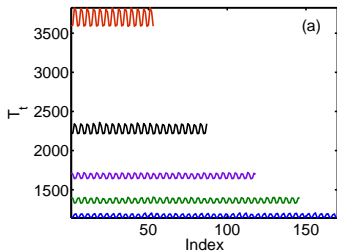
- (Left) Plot of the beat index versus the interbeat interval T_t for $\Omega = 15.3$(red curve), $\Omega = 15.8$(black curve), $\Omega = 16.3$(purple curve), $\Omega = 16.8$(green curve), and $\Omega = 17.3$(blue curve).

- (Right) Plot of the time averaged T_t for different values of Ω.
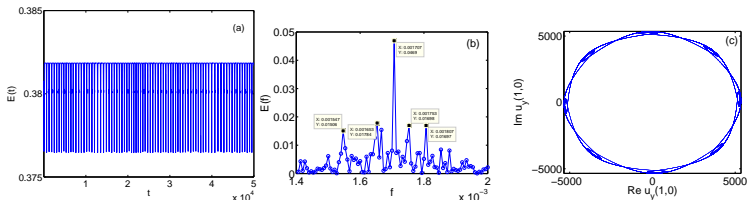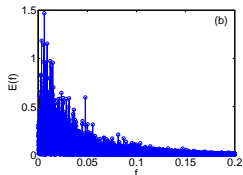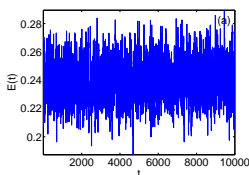
- ▶ (Left) The time evolution of the energy.
- ▶ (Middle) The frequency spectrum of the energy shows signature of quasi-periodic orbit + chaos.
- ▶ (Right) The plot of projection of the trajectory on the Fourier plane made by velocities $Re\hat{u}_y(1,1)$ versus $Im\hat{u}_y(1,1)$ shows formation of a new attractor.
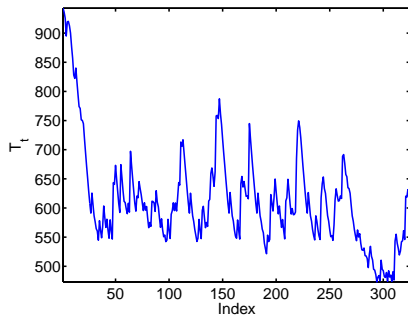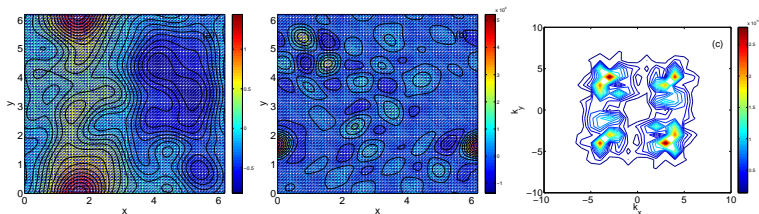
- Although $E(t)$ looks periodic, interbeat interval clearly shows a non-periodic behavior.
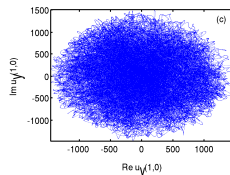
- (Left) $E(t)$ becomes chaotic.
- (Middle) $E(f)$ shows large number of frequencies getting excited.
- (Right) plot of projection of the trajectory on the Fourier plane made by velocities $Re[\hat{u}_y(1,1)]$ versus $Im[\hat{u}_y(1,1)]$.

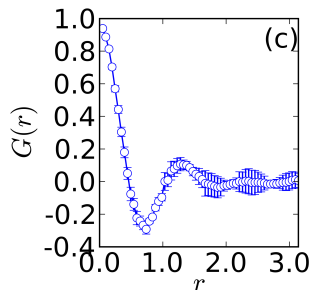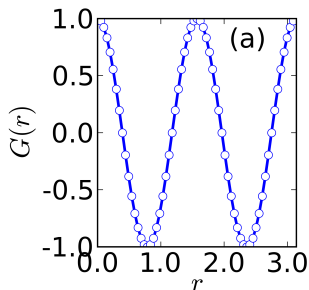# $\Omega = 50$: ψ, Λ, and E_Λ

- ▶ (Left) The streamfunction field.
- ▶ (Middle) The Λ field with superimposed contour lines.
- ▶ (Right) The plot of the reciprocal space energy spectrum E_Λ.

Auto-correlation function

$$G(r) = \langle \Lambda(\mathbf{x})\Lambda(\mathbf{x} + r) \rangle \qquad (7)$$

- ▶ Crystalline state: Peaks at lattice spacings.
- ▶ Liquid state: Peaks flatten.

Auto-correlation function

- Plots of $G(r)$:
  - (a) crystalline state : $n = 4$; $\Omega < \Omega_{s,n}$;
  - (c) circularly averaged in the turbulent state: $n = 4$; $\Omega = 20.81$.
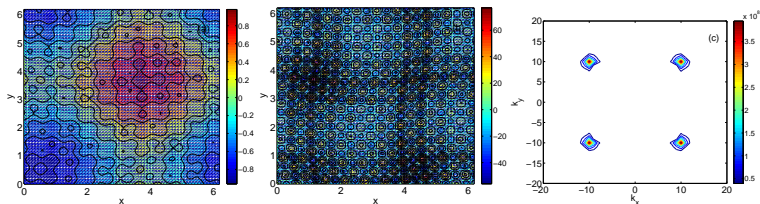
Results for n=10

	n	Ω	Comments
R10 − 1	10	$\Omega < \Omega_s$	Square array
R10 − 2	10	$\Omega_s < \Omega < 22.6$	Steady state
R10 − 3	10	$24 < \Omega < 28$	Periodic orbits
R10 − 4	10	$\Omega \geq 29$	Chaotic

Table: Table indicating the values of Ω and the route to chaos observed in our simulations.

- First steady state after $\Omega > \Omega_c$
- Pseudocolor plot of the streamfunction field.
- Pseudocolor plot of the Λ field.
- Contour plot of the reciprocal space energy spectrum E_Λ.

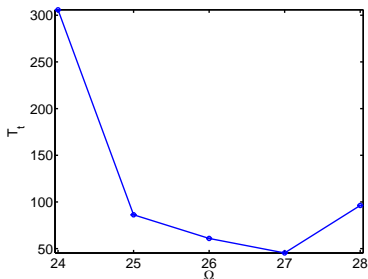# $\Omega = 24$: $E(t)$, $E(f)$, and Poincare section
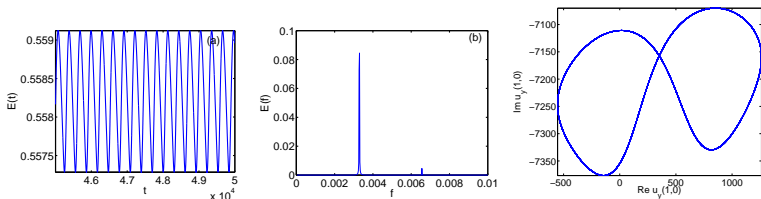
- ▶ (Left) The time evolution of the energy.
- ▶ (Middle) The frequency spectrum of the energy.
- ▶ (Right) The plot of projection of the trajectory on the Fourier plane made by velocities $Re\hat{u}_y(1,1)$ versus $Im\hat{u}_y(1,1)$.
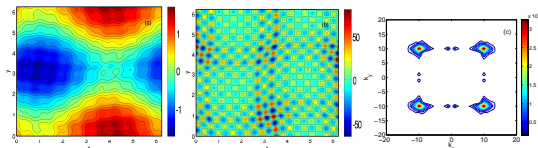
- Pseudocolor plot of the streamfunction field.
- Pseudocolor plot of the Λ field.
- Contour plot of the reciprocal space energy spectrum E_Λ.

Interbeat interval

- ▶ The interbeat interval $< T_t >$ first decreases on increasing Ω and then increase mildly at $\Omega = 28$.
- ▶ At $\Omega = 28$ the time-series is till periodic but now primary frequency around $f = 1$ and frequency at $f = 2, 3$ are also excited.
- ▶ $\Omega = 24$ the large structures in the streamfunction make oscillations around their mean positions.
- ▶ For $\Omega = 25$ to $\Omega = 28$ a travelling wave type solution is observed in the time evolution of the streamfunction.

$\Omega = 225$: $E(t)$, $E(f)$, and Poincare section
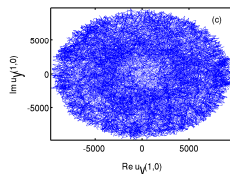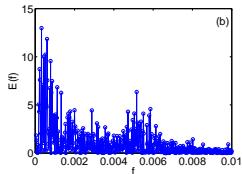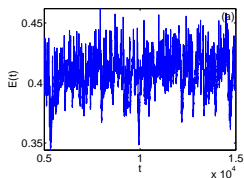
- ▶ (Left) The time evolution of the energy.
- ▶ (Middle) The frequency spectrum of the energy.
- ▶ (Right) Plot of projection of the trajectory on the Fourier plane made by velocities $Re[\hat{u}_y(1,1)]$ versus $Im[\hat{u}_y(1,1)]$.

Auto-correlation function
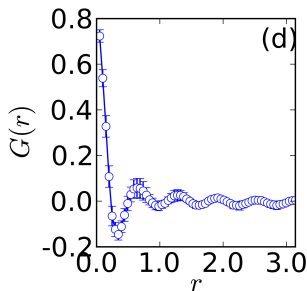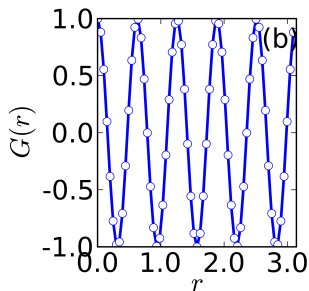
- Plots of $G(r)$:
  - (b) crystalline state : $n = 10$; $\Omega < \Omega_{s,n}$;
  - (d) circularly averaged in the turbulent state: $n = 4$; $\Omega = 225$.

Conclusions

- Transition to turbulence can be characterized by measures from density functional theory, non-linear dynamics, and turbulence.

- We have mapped in detail the transition to turbulence for these nonequilibrium systems.

Polymer Additives in Turbulent Flow

Drag Reduction

- Toms (1946): Monochlorobenzene with 0.25% (by weight) of polymethylmethacrylate
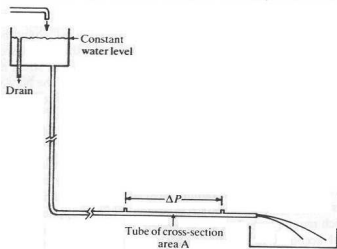
- Reduction in the pressure gradient across the pipe, on the addition of polymers, for the same volumetric flow rate
- Drag Reduction(in percentage) $DR \equiv \left(\frac{\Delta P_s - \Delta P_p}{\Delta P_s} \right) \times 100$

Reduction of small scale structures

- Turbulent jet of water with 50ppm polyethylene oxide at $Re \sim 225$
  [Turbulence structure in a water jet discharging in air, J.W. Hoyt and J.J. Taylor, Phys. Fluids, **20**, S253 (1977).]
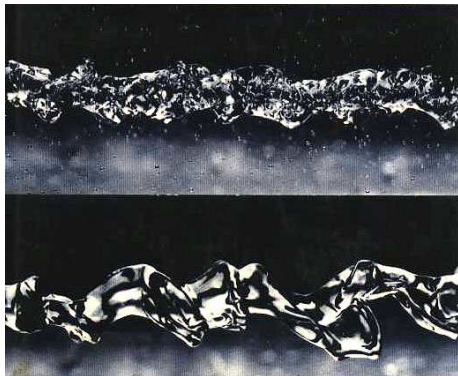
Eigenvalues of the strain tensor

[A. Liberzon, et al., Phys. Fluids, **17**, 031701 (2005).]
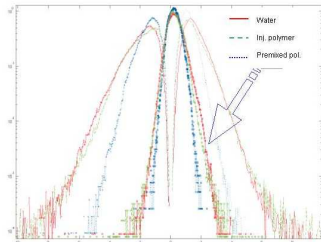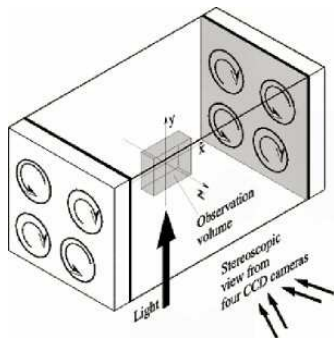
- Length:140mm, Width:120mm, Disk Dia.:40mm, Observation volume:$10 \times 10 \times 10mm$, $Re_\lambda = 38$.
- Regions of large strains reduced on the addition of polymers.

Structure function: $S_2(r)$

N.T. Ouellette, H. Xu, and E. Bodenschatz, ICTR website, (2007).
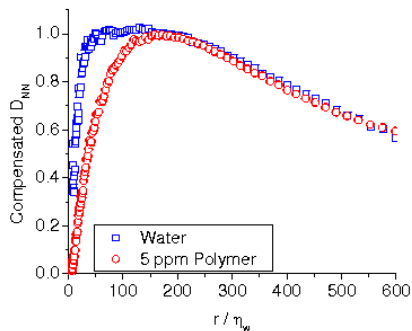
- $c = 5ppm, Re_\lambda = 290, Wi = 3.5$,
- Small scale structures are modified on the addition of polymers.

Polymer Properties

Typical drag-reducing polymer:

Polyethylene oxide $N \times$[-CH_2-CH_2-O-]

- Degree of polymerization (N) $\simeq 10^4$
- Molecular weight $\simeq 4 \times 10^6$ amu
- Zimm relaxation time $\simeq 10^{-4}$s
- RMS end-to-end distance at maximal extension $\simeq 34 \mu m$

Modelling polymer solutions

- Navier-Stokes(NS) with Polymer Additives:
  3D, unforced, incompressible, NS with additional stress because of polymers:

$$\frac{\partial \mathbf{u}}{\partial t} + (\mathbf{u} \cdot \nabla)\mathbf{u} = -\nabla p + \nu \nabla^2 \mathbf{u} + \nabla \cdot \mathcal{T},$$

where

- $\mathbf{u}(\mathbf{x}, t)$: fluid velocity; point $\mathbf{x}$; time t;
- ν: Kinematic viscosity of the fluid;
- $\mathcal{T}$: polymer contribution to the fluid stress;

$\nabla \cdot \mathbf{u} = 0$ enforces incompressibility.

Modelling polymer solutions:

- Polymer idealized as an elastic dumbbell with the non-linear force-extension relation

$$\mathbf{F} = \frac{H(L^2 - 3)}{(L^2 - r^2)}\mathbf{R}, \ r^2 < L^2,$$

where
  - $\mathbf{R}$: end-to-end displacement vector;
  - $r^2 = \langle \mathbf{R} \cdot \mathbf{R} \rangle$; $\langle \rangle$ indicates an average over polymer configurations;
  - H: spring constant;
  - L: maximum polymer extension.

Modelling polymer solutions:

► Polymer contribution to fluid stress

$$\mathcal{T}_{\alpha\beta} = \frac{\mu}{\tau_{poly}}\left(\frac{L^2-3}{L^2-\mathcal{C}_{\gamma\gamma}}\right)(\mathcal{C}_{\alpha\beta}-\delta_{\alpha\beta})$$
$$[\mathcal{C}_{\alpha\beta} \equiv \langle R_\alpha R_\beta\rangle]$$

where
  ► τ_{poly}: polymer relaxation time;
  ► μ: polymer viscosity parameter;
  ► $\mu/\tau_{poly} = nk_B T/N$;
  ► n: number of polymers per unit volume;
  ► N: number of monomer units constituting the polymer;
  ► k_B: Boltzmann constant; T is the temperature;
  ► L: Maximum polymer extension.

Modelling polymer solutions:

- Finitely Extensible Nonlinear Elastic-Peterlin(FENE-P) model

$$\frac{\partial \mathcal{C}_{\alpha\beta}}{\partial t} + (u_\gamma \partial_\gamma)\mathcal{C}_{\alpha\beta} = (\partial_\gamma u_\alpha)\mathcal{C}_{\gamma\beta} + \mathcal{C}_{\alpha\gamma}(\partial_\gamma u_\beta) - \frac{1}{\mu}\mathcal{T}_{\alpha\beta}.$$

["Dynamics of polymeric liquids", Bird, *et al.*]

- $c = \mu/(\nu + \mu)$; $c = 0.1 \simeq 100 ppm$ of PEO
- $We = \tau_{poly}\sqrt{(\epsilon(t_m)/\nu)}$; t_m is the time corresponding to the peak in ϵ for $c = 0$

[Vaithianathan, *et al.*, JCP, **187**, 1 (2003).]

Solve NS and FENE-P numerically

$$\frac{\partial u_\alpha}{\partial t} + (u_\gamma \partial_\gamma)u_\alpha = -\partial_\alpha p + \nu \partial_{\gamma\gamma} u_\alpha + \partial_\gamma \mathcal{T}_{\alpha\gamma},$$
$$\partial_\gamma u_\gamma = 0,$$

$$\frac{\partial \mathcal{C}_{\alpha\beta}}{\partial t} + (u_\gamma \partial_\gamma)\mathcal{C}_{\alpha\beta} = (\partial_\gamma u_\alpha)\mathcal{C}_{\gamma\beta} + \mathcal{C}_{\alpha\gamma}(\partial_\gamma u_\beta) - \frac{1}{\mu}\mathcal{T}_{\alpha\beta}.$$

Integrating the NS equation

- Use second-order Adams-Bashforth scheme for time marching
- Integrate viscous term exactly in Fourier space
- Non-linear terms calculated in velocity-vorticity formulation
- The polymer contribution to the fluid stress added to the non-linear terms
- Use 2/3-dealiasing method to remove the aliasing error

$$u^{n+1} = \exp(-\nu k^2 \delta t)u^n + \frac{1 - \exp(-\nu k^2 \delta t)}{\nu k^2}P_{ij}[(3/2)N^n - (1/2)N^{n-1}]$$

where

- n: iteration number;
- N: sum of the non-linear and the polymer stress term $(\mathbf{u} \times \omega) + \nabla \cdot \mathcal{T}$ in Fourier space;
- $P_{ij} = (\delta_{ij} - k_i k_j / k^2)$

[A. Vincent and M. Meneguzzi, JFM, **225**, 1 (1991).]

- ▶ A second-order Adams-Bashforth scheme is used for time marching
- ▶ Use sixth-order centered finite-difference scheme for calculating derivatives in space

- Loss of SPD nature of $\mathcal{C}$ during numerical integration $\Rightarrow$ negative eigenvalues(Hadamard instability)
- Because of numerical errors r^2 can become $\geq L^2$. This leads to numerical blowup of the elements of $\mathcal{C}$.

Integrating the FENE-P equation: Remedies

Conserving SPD nature of $\mathcal{C}$, Cholesky decomposition:

- Define $\mathcal{J} = \frac{L^2-3}{L^2-r^2}\mathcal{C}$
- Define $\mathcal{J} = \mathcal{L}\mathcal{L}^{\mathcal{T}}$ where $\mathcal{L}$ is a lower-triangular matrix with elements ℓ_{ij}
- Solve
  $$D_t\ell_{i1} = \sum_k \Gamma_{ki}\ell_{k1} + \frac{1}{2}\left[(q-s)\ell_{i1} + (-1)^{(i \bmod 1)}\frac{s\ell_{i1}}{\ell_{11}^2}\right]+$$
  $$(\delta_{i,3}+\delta_{i,2})\frac{\ell_{i1+1}}{\ell_{11}}\sum_{m>1}\Gamma_{m1}\ell_{m2}+$$
  $$\delta_{i,3}\Gamma_{i1}\frac{\ell_{33}^2}{\ell_{11}}, \text{ for } i \geq 1;$$

Integrating the FENE-P equation: Remedies

$$D_t \ell_{i2} = \sum_{m \geqslant 2} \Gamma_{mi} \ell_{m2} - \frac{\ell_{i2-1}}{\ell_{11}} \sum_{m \geqslant 2} \Gamma_{m1} \ell_{m2} +$$
$$\frac{1}{2} \left[(q-s)\ell_{i2} + (-1)^{(i+2)} s \frac{\ell_{i2}}{\ell_{22}^2} \left(1 + \frac{\ell_{21}^2}{\ell_{11}^2} \right) \right] +$$
$$\delta_{i,3} \left[\frac{\ell_{33}^2}{\ell_{22}} \left(\Gamma_{32} - \Gamma_{31} \frac{\ell_{21}}{\ell_{11}} \right) + s \frac{\ell_{21} \ell_{31}}{\ell_{11}^2 \ell_{22}} \right], \text{ for } i \geq 2;$$

$$D_t \ell_{33} = \Gamma_{33} \ell_{33} - \ell_{33} \left[\sum_{m<3} \frac{\Gamma_{3m} \ell_{3m}}{\ell_{mm}} \right] + \frac{\Gamma_{31} \ell_{32} \ell_{21} \ell_{33}}{\ell_{11} \ell_{22}} -$$
$$s \frac{\ell_{21} \ell_{31} \ell_{32}}{\ell_{11}^2 \ell_{22} \ell_{33}} + \frac{1}{2} \left[(q-s)\ell_{33} + \right.$$
$$\left. \frac{s}{\ell_{33}} \left(1 + \sum_{m<3} \frac{\ell_{3m}^2}{\ell_{mm}^2} \right) + \frac{s \ell_{21}^2 \ell_{32}^2}{\ell_{11}^2 \ell_{22}^2 \ell_{33}} \right].$$

SPD nature of $\mathcal{C}$ guaranteed by construction.

- $s = (L^2 - 3 + j^2)/(\tau_{poly} L^2)$,
- $q = [d/(L^2 - 3) - (L^2 - 3 + j^2)(j^2 - 3)/(\tau_{poly} L^2 (L^2 - 3))]$,
- $j^2 \equiv Tr(\mathcal{J})$, and $d = Tr[\mathcal{J}.(\nabla \mathbf{u}) + (\nabla \mathbf{u})^T.\mathcal{J}]$.
  [Vaithianathan, et al., op. cit.]

- Increase of r^2 beyond L^2: Controlled only by reducing the time-step.

CPU Resources and Memory requirements

- MPI-version of the code developed.
- A complete 256^3 decaying DNS generates 120GB of data.
- A 512^3 DNS of NS+FENE-P requires 21GB of RAM.

Memory Requirements

- DNS of NS+FENE-P: Requires 3 times more RAM than the DNS of NS.
- Estimated RAM for 2048^3 DNS of NS+FENE-P: 1344GB!

Results: Initial Condition

- Start from an initial energy spectrum with energy concentrated in the first few Fourier modes and the polymers unstretched

- Monitor the decay of the energy dissipation rate and the energy spectrum for the fluid with and without polymer additives.

Energy Dissipation Rate

$N = 256$, $\nu = 10^{-3}$, $\tau_{poly} = 1$
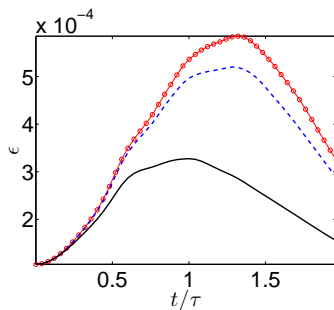
- The energy dissipation rate $\epsilon(t)$ as a function of time t for different values of c.
- The peak in $\epsilon(t)$ decreases as c increases.

Dissipation Reduction(DR)

$N = 96$, $\nu = 10^{-2}$
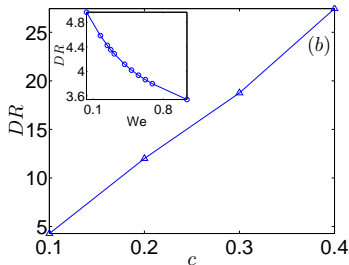
- Natural definition of dissipation-reduction
  $\%DR = \left(\frac{\epsilon^{f,m} - \epsilon^{p,m}}{\epsilon^{f,m}} \right) \times 100;$
- f and p stand, respectively, for the fluid without and with polymers.
- An increase in c enhances the dissipation reduction DR (cf., earlier shell-model study).
- DR decreases marginally with an increase in *We*.

Fluid energy spectrum

$N = 192$, $\nu = 10^{-2}$, $\tau_{poly} = 1$
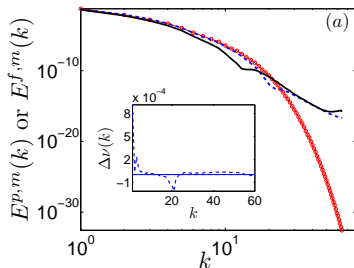
- $E_f(k) = \sum_{k-1/2 < k' < k+1/2} |\mathbf{u}(k')|^2$ at t_m for polymer concentrations $c = 0$(o-), $c = 0.1$(–) and $c = 0.4$(-).
- Energy spectrum at cascade completion changes significantly for large Fourier modes.
- This had not been resolved by earlier, high-Re simulations!

Scale-dependent viscosity

$N = 192$, $\nu = 10^{-2}$, $\tau_{poly} = 1$
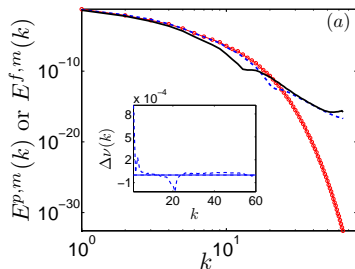
- The change in the spectra and ϵ can be understood in terms of an additional, effective, scale-dependent viscosity $\Delta\nu(k) \equiv -\mu \sum_{k-1/2 < k' \le k+1/2} \mathbf{u}_{\mathbf{k}'} \cdot (\nabla \cdot \mathcal{J})_{-\mathbf{k}'}/[\tau_{poly} k'^2 E^{p,m}(k')]$.
- Since $\Delta\nu$ becomes negative, polymers pump energy into the fluid around $k \simeq 10$.

Structure Functions

Order-p equal-time, longitudinal velocity structure function.

$$\begin{aligned}
\mathcal{S}_p(r) &\equiv \langle \delta u(r, t)^p \rangle, \\
\delta u_\parallel(r, t) &\equiv [\vec{u}(\vec{x} + \vec{r}, t) - \vec{u}(\vec{x}, t)] \cdot (\vec{r}/r).
\end{aligned}$$

Second order structure function $S_2(r)$

Experiments(Ouellette, et al.)
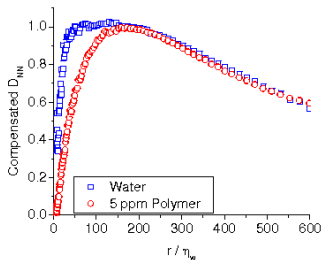
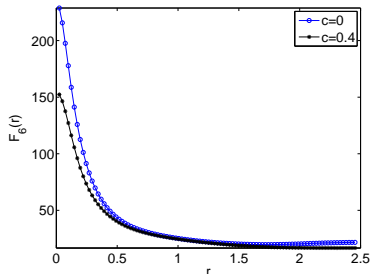Figure: $c = 5ppm$, $Re_\lambda = 290$, and $We = 3.5$

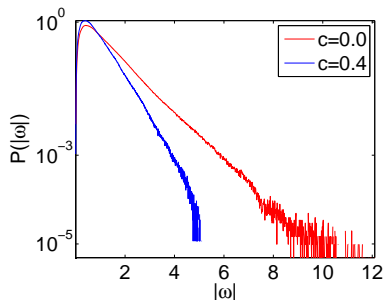Our DNS
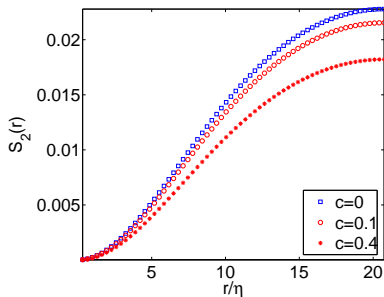
Figure: $N = 128$, $\nu = 0.01$, and $\tau_P = 1.5$

Hyperflatness:

$N = 192$, $\nu = 10^{-2}$, $\tau_{poly} = 1$

- Hyperflatness: $F_6(r) = \dfrac{\mathcal{S}_6(r)}{(\mathcal{S}_2(r))^3}$.
- Polymers slow down the unbounded growth in $F_6(r)$ at small r, i.e., small-scale intermittency decreases.

PDF of |ω|

- Probability distribution of the modulus of the vorticity($P(|\omega|)$) at cascade completion($c=0$, $c=0.4$).
- Addition of polymers leads to a decrease in the regions of large vorticity.

Isosurfaces of $|\omega|$

$N = 256$, $\nu = 10^{-3}$, $\tau_{poly} = 1$
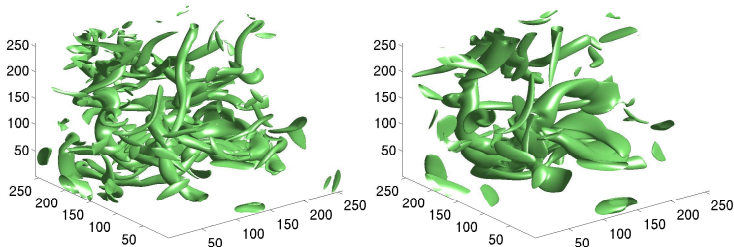
- Iso-$|\omega|$ surfaces for $|\omega| = \langle |\omega| \rangle + 2\sigma$ for $c = 0$(left) and $c = 0.4$(right) at t_m.

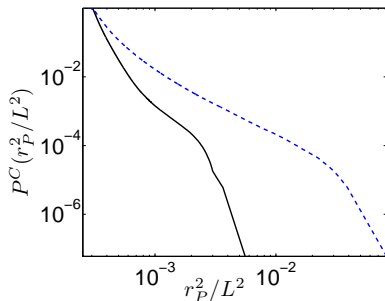- Small-scale structures are suppressed on the addition of polymers.

PDF of Λ_1
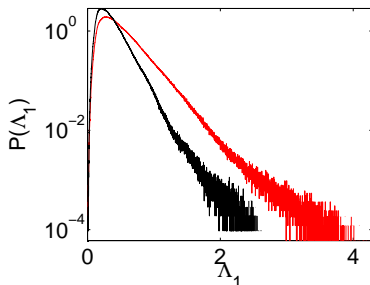
- PDF of the largest eigenvalue(Λ_1) of the rate of strain tensor($S_{ij} = (\partial_i u_j + \partial_j u_i)/2$) at cascade completion(c=0, c=0.4).
- The addition of polymers leads to a decrease in the regions of large strains.

Stretching of Polymers:Cumulative distribution(CDF)

$N = 256$, $\nu = 10^{-3}$, $\tau_{poly} = 1$

- $c = 0.1$(dashed line), $c = 0.4$(line).
- An increase in c leads to a decrease in the polymer extension.
- A decrease in ν leads to turbulent flows and large polymer extensions.

Forcing

- Stochastic forcing of V. Eswaran and S.B. Pope, Computers and Fluids, **16**, 257 (1988)
- Force all the Fourier modes with $k \leq \sqrt{2}$
- Forcing is done by a vector-valued Ornstein-Uhlenbeck stochastic diffusion process with variance σ^2 and time-scale T_L
- $\langle \tilde{\mathbf{f}}(\mathbf{k}, t) \rangle = 0$
- $\langle \tilde{\mathbf{f}}(\mathbf{k}, t) \tilde{\mathbf{f}}^*(\mathbf{k}, t + s) \rangle = 2\sigma^2 \mathbb{I} \exp(-s/T_L)$
- Here the angular brackets denote ensemble averages, an asterisk denotes complex conjugate, $\mathbb{I}$ is the identity tensor

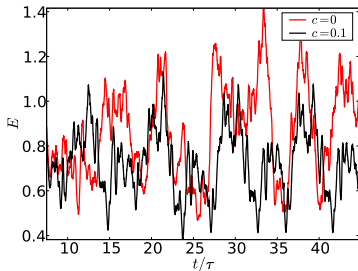# Energy dissipation rate

$N = 64$, $Re_\lambda = 9.91$, $L = 100$
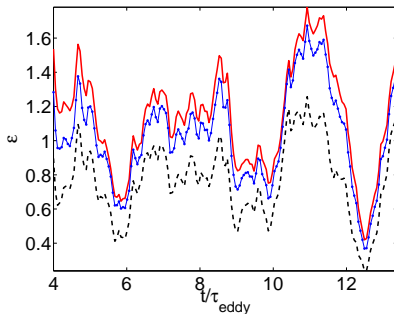
- Time-averaged ϵ decreases with an increase in the polymer concentration($c = 0(–)$, $c = 0.1(.–)$, and $c = 0.33(—)$)), at fixed $We = 1.17$
- Small-time behavior same as for decaying turbulence
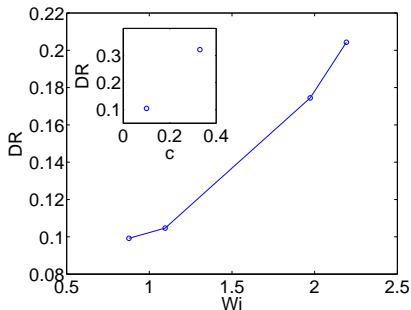
Time evolution of E and ϵ

$N = 512$, $Re_\lambda \simeq 23$, $We = 1.5$
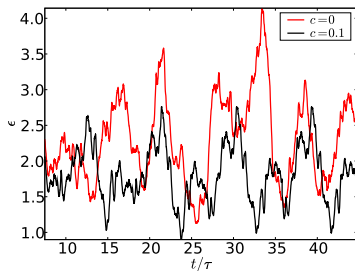
- Time averaged E decreases with an increase in c
- Time averaged ϵ decreases with an increase in c
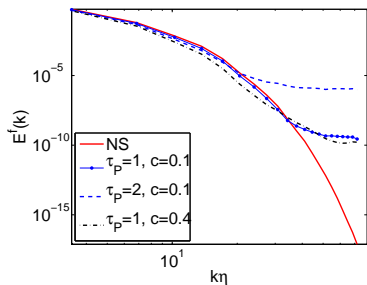- In agreement with our studies on decaying turbulence

Dissipation Reduction

- Natural definition of dissipation reduction
  $\%DR \equiv \frac{\bar{\epsilon}_f - \bar{\epsilon}_p}{\bar{\epsilon}_f} \times 100$: the overbar indicates time averaging
- f and p stand, respectively, for the fluid without and with polymers.
- DR increases with an increase in: (a) c at fixed We; (b) We at fixed c

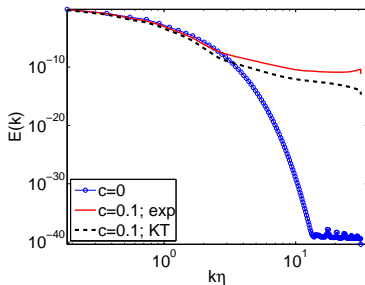# Energy spectrum

Left: $N = 64$ Right: $N = 512$

- Unlike earlier studies we have a fully resolved deep-dissipation range
- Energy spectra are similar to those in our DNS of decaying turbulence

Second order Structure function $S_2(r)$

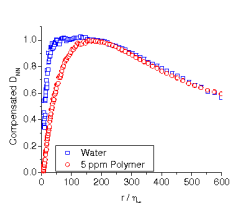Experiments(Ouellette et al.)   Our DNS
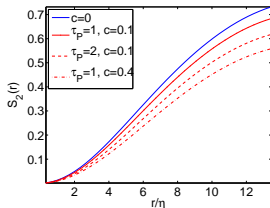

Figure: $c = 5ppm$, $Re_\lambda = 290$, and $We = 3.5$
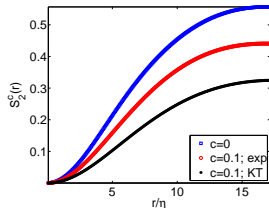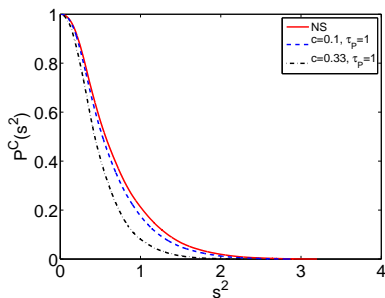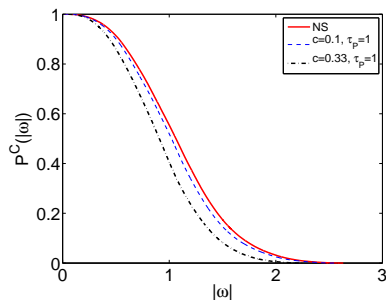
Figure: $N = 64$, $Re_\lambda = 9.09$, and $We = 1.17$

Figure: $N = 512$, $Re_\lambda \simeq 23$, and $We = 1.5$

- ▶ $S_2(r) \equiv \int_0^\infty (1 - \sin(kr)/kr)E(k)dk$
- ▶ Compensated structure function:
  $S_2^c(r) = [(3/4)S_2(r)/2.13]^{3/2}/(\epsilon r)$
- ▶ Note similarity with experiments.

Cumulative distribution function of s^2 and ω^2
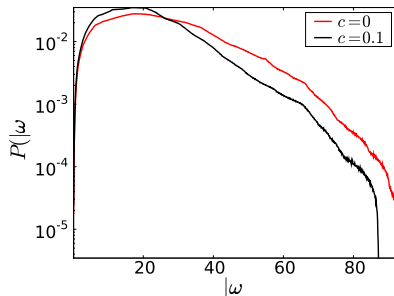
$N = 64$, $Re_\lambda = 9.09$, and $We = 1.17$

- $\omega^2 \equiv \sum_{i,j} \omega_{ij}\omega_{ij}$, $s^2 \equiv \sum_{i,j} s_{ij}s_{ij}$, $s = (\nabla\mathbf{u} + (\nabla\mathbf{u})^T)/2$, $\omega = \nabla \times \mathbf{u}$

- Regions of large strain and vorticity decrease on the addition of polymers

PDF of |ω|

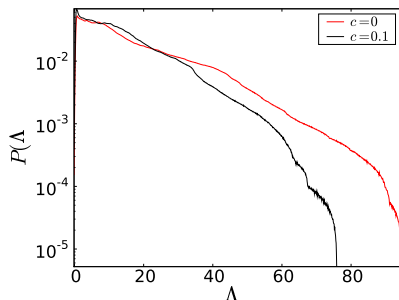$N = 512$, $Re_\lambda \simeq 23$, $We = 1.5$, $c = 0.1$

- Probability distribution of the modulus of the vorticity($P(|\omega|)$) (c=0, c=0.1).
- Addition of polymers leads to a decrease in the regions of large vorticity.

PDF of Λ
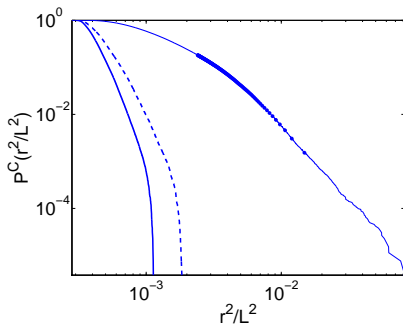
$N = 512$, $Re_\lambda \simeq 23$, $We = 1.5$, $c = 0.1$

▶ Regions of large strain reduced on the addition of polymers.

Polymer extensions

$N = 64$

- $We = 2.34$, $c = 0.1$(.–); $We = 1.17$, $c = 0.1$(dashed line); $We = 1.17$, $c = 0.33$(line)
- Polymer extensions larger in comparison to decaying turbulence
- At fixed c, polymer extension increases with an increase in We
- At fixed We, polymer extension decreases with an increase in c

Conclusions

- Turbulence is complex in several ways.

- Turbulence displays emergent behaviour in the form of coherent structures.

- It exhibits complicated, disordered spatiotemporal behaviours.

- Equal-time and time-dependent structure functions show power-law behaviours like correlation functions at a critical point in, say, a magnet.

- Simple scaling, as in most critical phenomena, must be replaced by multiscaling.

Conclusions

- Velocity structure functions in two-dimensional turbulence show simple scaling but their vorticity counterparts display multiscaling.

- Polymer additives lead to drag and dissipation reduction in turbulent flows.

- They also suppress small-scale structures.

- State-of-the-art experiments, high-performance computing, and theory must go hand-in-hand to characterise the complexity of turbulence.